JOURNAL OF SOLID STATE CHEMISTRY 53, 329–343 (1984)

A Theoretical Model of Solid State Phase Reactions: Hysteresis and Kinetics

A. MAREN,* S. H. LIN,† R. H. LANGLEY,‡ AND L. EYRING

Department of Chemistry, Arizona State University, Tempe, Arizona 85287

Received March 5, 1984

Hysteresis in the pressure-dependent solid state phase transition Pr_7O_{12}–Pr_9O_{16} is modeled using a thermodynamic formalism. The system is considered to be formed of a fixed number of domains, which are differentiated on the basis of size. The two cases of noninteracting and interacting domains are considered. The interacting domains model allows a better fit to experimental results. In each case, the model is applied to four different isothermal hysteresis curves for the Pr_7O_{12}–Pr_9O_{16} phase transition. The kinetics of the phase transition are studied for the case of noninteracting domains.

I. Introduction

The phenomenon of hysteresis is found when a system follows one path in going from an initial state A to a final state B, and a different path when it undergoes the reverse transition from B to A. (In this paper the word "transition" is used whether or not the transformation is accompanied by a compositional change.) This phenomenon has been observed in many different types of systems, including electric-current and magnetic hysteresis (*1*), hysteresis in the phase transitions of solids (*2–4*), and even hysteresis in gas-phase reactions (*5*) and biological systems (*6*).

The theoretical formalism which has been developed to explain hysteresis draws on the concept of thermodynamically metastable states. In the normal course of phase transitions, the system is considered to be in a state defined by the lowest point on the free energy curve. (Here the free energy will be considered in statistical mechanical terms as a function of some intrinsic variable such as concentration.) Plots of reduced free energy (free energy divided by Boltzmann's constant and temperature) are shown in Fig. 1. At a low value of an external parameter, such as temperature or pressure, there is a single minimum in the reduced free energy curve, which represents the equilibrium concentration for that system. As the value of the external parameter is increased, a second minimum may form. This new minimum will increase in depth relative to the original one as the external parameter is increased, until at some value they are equal in depth. The two minima in the reduced free energy curves then represent two equilibrium states for the system, and the system should be able to undergo a phase transition.

The concept of metastable states invoked

* Present address: Systems and Research Center, Honeywell, Inc., 2600 Ridgway Parkway, Minneapolis, Minn. 55413.

† To whom inquiries should be made.

‡ Present address: Dept. of Chem., Stephen F. Austin State University, Nacogdoches, Tex. 75962.

0022-4596/84 $3.00

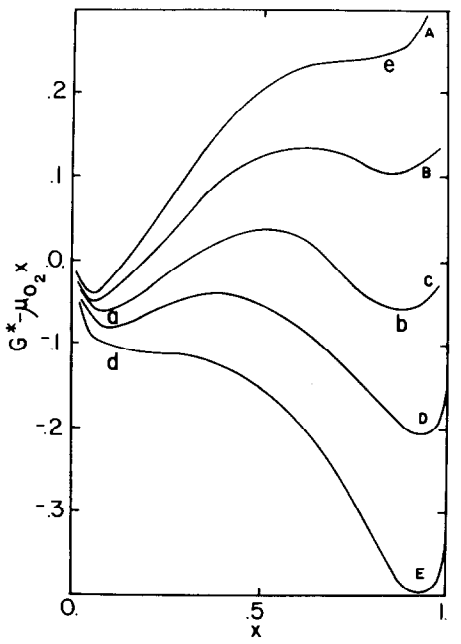

FIG. 1. Plots of reduced free energy, G^*, against concentration. Points *a* and *b* on curve C represent the equilibrium transition values for the system, and points *e* on curve A and *d* on curve E represent the hysteresis transition values for phases B and A, respectively.

for hysteresis postulates that the system does not undergo a transition at the point where the two states are in equilibrium. Instead, the system remains in the original state (phase A) through increasing values of the external variable until the minimum defining the new metastable phase disappears completely. Then the system presents no resistance to the energetically favorable transition to the new phase.

Although this approach is sufficient to describe the hysteresis of a system as a whole, there is evidence that systems that show hysteresis do not undergo the phase transitions all at once. Instead, domains or nuclei of the new phase, B, first appear in the original material, A (*4–7*). As the external parameter is changed further, the number and size of these domains increases until the system is finally composed solely of B. The reverse transition begins as the change in the external parameter is reversed, and domains of A appear in B.

Two major approaches have been used to model these observations. In one approach, the "nucleation and growth" theory, domains of B are seen as nucleating out of a parent material A (*7, 8*). The size distribution of domains of B is given as a function of the external parameter, and is also governed by a parameter which gives the interaction between the domains. The reverse transition follows a different path if different parameters are chosen for the interaction of domains of B in a parent material of A and for the interactions of domains of A in a parent material of B.

A difficulty with this approach is that it does not deal adequately with partially completed phase transitions. If the external parameter is reversed before the phase transition is complete, the original path would be retraced. However, it is known that if the external parameter is reversed, a hysteresis loop (scanning loop) appears.

The second approach, which was developed by Everett (*9*), and later expanded by Enderby (*10*), proposes that a system is divided into domains even before a phase transition begins. The number and size of these domains remains a constant. Each domain has an individual free energy, which depends on two or more intrinsic variables. As the external parameter changes, the domains will undergo phase transitions, each of which is determined by the free energy curve of the domain. The result is a series of domain phase transitions which yield an overall transition for the system.

In this investigation, a thermodynamic approach is used to model the free energy of individual domains within a system. Each domain is presumed to undergo a separate transition between the two phases, and each exhibits hysteresis in its phase transition. The model is applied to four iso-

thermal measurements of the pressure-dependent iota–zeta phase transition in praseodymium oxide (*11*):

$$Pr_9O_{16} \rightleftarrows \tfrac{9}{7}Pr_7O_{12} + \tfrac{2}{7}O_2$$

In Section II, the model is formulated for the case of noninteracting domains. The system is viewed one-dimensionally, where each domain is in direct contact with the external oxygen. The domains are of different widths, and are distinguished on the basis of a concentration gradient which is presumed to exist across the width of the domains (*12*). This concentration gradient affects the maxima and minima of the chemical potential, and consequently affects the pressures at which the domain undergoes its forward and reverse transitions.

The kinetics of the phase transition is also studied in Section II, using a theoretical treatment that is derived from the concepts of irreversible processes (*13*). The rate equation, based on Kikuchi's path probability theory (*14*), assumes the rate of change of the concentration to depend linearly on the distance of the system from equilibrium. Both first- and second-order approximations to the rate constant are calculated, and are compared with kinetic studies of the iota–zeta transition (*11*).

In Section III the approach is modified in such a way that a form of nucleation and growth is also incorporated. The domains are now considered to be in a two-dimensional array; each a unit cell in width but variable in length. (This is in accordance with the electron microscope images of the domains (*15*).) Interactions between the domains are posed such that there is no net interaction between like domains, but that if a domain in phase A undergoes a transition to B, the interaction between it and a nearest-neighbor domain in A will allow the nearest-neighbor to undergo a transition to B more readily than it would have otherwise. In this way, the initial transition may be viewed as a "nucleation" of phase B in the original phase A, and additional aided transitions of successive nearest-neighbor domains may be seen as "growth" of the original "nucleus." This treatment allows some unification of the two approaches that previously seemed quite different, the "nucleation and growth" concept and the theory of transitions of preexisting domains.

II. A Theoretical Model for a Solid State Phase Transition Using Noninteracting Domains

A. A Theoretical Model for Hysteresis in the Phase Transition

Following the proposals of Everett (*9*) and Enderby (*10*), the system is considered to be composed of a number of domains of various widths. The state of each domain depends on an extrinsic variable N_α. The free energy G_α of domain α depends on N_α, and the total free energy of the system may be expressed as

$$G = \sum_\alpha G_\alpha(N_\alpha). \tag{2.1}$$

The N_α's are clearly subject to the condition

$$\sum_\alpha N_\alpha = N_t, \tag{2.2}$$

where N_t is the total amount of N_α (e.g., the total excess oxygen present). The condition that these domains should be in thermodynamic equilibrium is obtained by minimizing G subject to the constraint

$$\frac{\partial G_\alpha}{\partial N_\alpha} = \lambda, \tag{2.3}$$

where λ is a Lagrange multiplier. Note that this is identical to the constraint

$$\frac{\partial G}{\partial N_t} = \lambda. \tag{2.4}$$

To apply Eqs. (2.1)–(2.4) to rare earth oxides, $G(N_\alpha)$ is formulated as G_{N_0}, the free

energy for a domain with N_0 excess oxygen atoms. Using the regular solution theory (*16*), G_{N_0} may initially be written as

$$G_{N_0} = \xi_0 N_0 + \frac{\xi_i N_0^2}{N} + k_B T \left[N_0 \ln \left(\frac{N_0}{N} \right) + (N - N_0) \ln \left(\frac{N - N_0}{N} \right) \right]. \quad (2.5)$$

In Eq. (2.5), ξ_0 is the enthalpy per excess atom, N the total number of sites available for excess atoms, and ξ_i the interaction energy between nearest-neighbor excess atoms. The enthalpy contribution for each excess atom is given in the first term, the interactive energy for a nearest-neighbor excess oxygen atom in the second term, and the entropy contribution for the randomly distributed atoms in the third term.

To introduce the size-dependent differentiation between domains, a theory developed by Cahn and Hilliard (*12*) for the interfacial free energy of a nonstoichiometric system is adapted to the system of domains. The local free energy, g, in a region with a concentration gradient may be expressed as a function of the concentration, x, the gradient of the concentration, ∇x, and derivatives of the gradient, $\nabla^2 x$. It is assumed that the change in concentration is small with respect to the reciprocal of the intermolecular distance,

$$g = g(x, \nabla x, \nabla^2 x, \ldots). \quad (2.6)$$

Expressing g as an expansion about the local free energy for an area without a concentration gradient (g_0), we obtain

$$g = g_0 + K_1(\nabla x)^2 + K_2 \nabla^2 x, \quad (2.7)$$

where

$$K_1 = \frac{1}{2} \frac{\partial^2 g}{\partial \nabla x^2} \quad \text{and} \quad K_2 = \frac{\partial g}{\partial (\nabla^2 x)}, \quad (2.8)$$

and the first-order term has been dropped due to symmetry considerations (using the approximation of a cubic crystal).

Following Cahn and Hilliard, the free energy for the entire domain may be expressed by integrating the local free energy over the volume of the domain,

$$G = x\int g_0 dV + x\int K_1(\nabla x)^2 dV + x\int K_2(\nabla^2 x) dV. \quad (2.9)$$

The first term on the right-hand side is given in Eq. (2.5). The third term may be simplified by use of the divergence theorem, and by setting the resultant surface integral equal to zero. The second and third terms may then be combined to yield (*12*)

$$G = G_0 + x\int K(\nabla x)^2 dV. \quad (2.10)$$

The second term, which is due to the concentration gradient, may be evaluated by assuming that ∇x may be approximated as the constant ratio $\Delta x/w$, where w is the width of a domain. Notice that

$$K = K_1 - \frac{\partial K_2}{\partial x}.$$

The total free energy expression for a domain may now be written as

$$G = \xi_0 N_0 + \frac{\xi_i N_0^2}{N} + N_0 \frac{K}{w^2} (x - x_e)^2 + k_B T \left[N_0 \ln \left(\frac{N_0}{N} \right) + (N - N_0) \ln \left(\frac{N - N_0}{N} \right) \right], \quad (2.11)$$

where x_e is the equilibrium concentration. Dividing Eq. (2.11) through by N yields the free energy per site for excess oxygen atoms,

$$\bar{G} = \frac{G}{N} = \xi_0 x + \xi_i x^2 + Kx(x - x_e)^2/w^2 + k_B T[x \ln x + (1 - x) \ln(1 - x)]. \quad (2.12)$$

The chemical potential of the oxygen atoms can be calculated from Eq. (2.12) as

$$\mu_O = \frac{\partial \bar{G}}{\partial x} = \xi_0 + 2\xi_i x + \frac{K}{w^2}(3x^2 - 4xx_e + x_e^2) + k_B T \ln\left(\frac{x}{1-x}\right). \quad (2.13)$$

At thermal equilibrium,

$$\mu_O = \tfrac{1}{2}\mu_{O_2} = \tfrac{1}{2}(\mu^0_{O_2} + k_B T \ln P_{O_2}), \quad (2.14)$$

where μ_{O_2} represents the chemical potential of O_2 in the gas phase, and $\mu^0_{O_2}$ represents the standard chemical potential of O_2 in the gas phase. Combining Eq. (2.14) with Eq. (2.13),

$$P_{O_2}^{1/2} K_0(T) = \frac{x}{1-x} \exp\left[\frac{2\xi_i x + K(3x^2 - 4xx_e + x_e^2)/w^2}{k_B T}\right], \quad (2.15)$$

where

$$K_0(T) = \exp\left(\frac{\tfrac{1}{2}\mu^0_{O_2} - \xi_0}{k_B T}\right). \quad (2.16)$$

B. Application of the Model to the Pr_7O_{12}–Pr_9O_{16} Phase Transition

To demonstrate the behavior of Eq. (2.15), it is expressed in the reduced form

$$P^{*1/2}_{O_2} = \frac{x}{1-x} \exp[-2x + K^*(3x^2 - 4xx_e + x_e^2)]/T^*, \quad (2.17)$$

where

$$P^{*1/2}_{O_2} = P^{1/2}_{O_2} K_0(T)$$
$$T^* = -k_B T/\xi_i$$
$$K^* = -K/\xi_i w^2. \quad (2.18)$$

The plot of $P^{*1/2}_{O_2}$ versus x is similar in form to plots of μ versus x and P_{O_2} versus x. The maxima and minima for the $P^{*1/2}_{O_2}$ curve occur at the same values of x as the maxima and minima of the P_{O_2} and μ curves.

The points on the pressure versus concentration curve (Fig. 2) represent the minima (or maxima) for the free energy. Thus, a point (P_{O_2}, x) represents a particular solution of the free energy equation minimized with respect to concentration. In the region where there are two minima, there are three possible values of x for a given value of P_{O_2}. Only the largest and smallest values for x are physically realizable; the middle value corresponds to an instability in the free energy curve (the maxima separating two minima).

The maximum on the pressure versus concentration curve (Fig. 2) represents the highest value of pressure for which the system can remain in phase A. Similarly, the minimum on the curve represents the lowest possible value of pressure the system in phase B can hold before a transition to phase A is induced.

Figure 2 represents the nature of the system without domain considerations. Figure

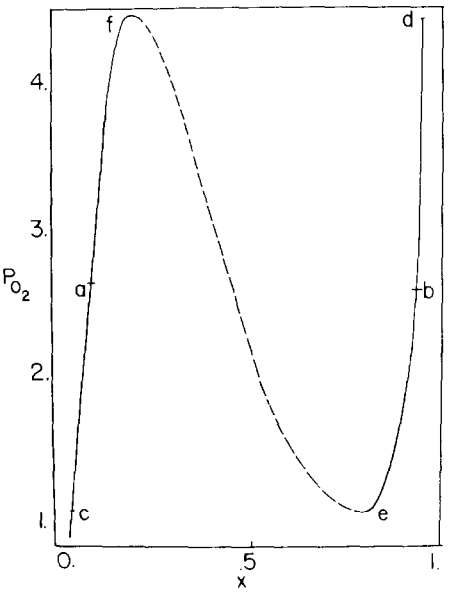

FIG. 2. Oxygen pressure (in Torr) against concentration, calculated for the Pr_7O_{12}–Pr_9O_{16} phase transition at 550°C. Points *a* and *b* are the points where the phases A and B are in equilibrium with each other. The hysteresis phase transitions occur at points *e* and *f*.

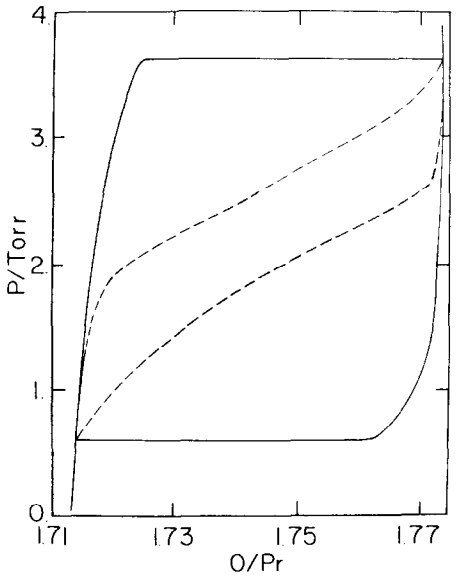

FIG. 3. Calculated fit to the hysteresis curve at 550°C, without use of domains. The broken lines represent the experimental results.

3 illustrates the calculated fit to the hysteresis curve at 550°C without use of domains. The poor fit achieved with the bulk approach emphasizes the need for a domain approach such as adopted here.

To incorporate the effect of domains, the two parameters K^* and x_e have been introduced. K^* is the basis for distinguishing the chemical potential of domains of different lengths, and hence for providing different P_{O_2} versus concentration curves. Recall that $K^* = -K/(\varepsilon_i w^2)$, so that K^* is proportional to K, which is related to the dependence of the local free energy of a domain on the concentration of excess oxygen atoms (Eqs. (2.9) and (2.10)). Further, K is inversely proportional to ε_i (the interaction energy between excess oxygen atoms) and to w^2. Overall, it is the dependence of K^* on w^2 which is most significant. Since K^* is inversely proportional to the square of the width of a domain, it is clear that when the system as a whole is considered to be one very large domain, w^2 is very large and the contribution of terms involving K^* is negligible. This corresponds to the bulk hysteresis case. For small values of w, the influence of K^* on the chemical potential is quite noticeable. As the values used for K^* are negative, the influence of the K^* terms is to lower the maxima and raise the minima. This means that the smallest domains (with the largest magnitude of K^*) will have the lowest maxima, and hence be the first to undergo transition to the new phase. They will be followed by transitions of domains of increasing size as the pressure is raised. Similarly, the smallest domains will also have the highest minima and will be the first to undergo reverse transitions to phase A. These effects are illustrated in Fig. 4.

To fit the experimental hysteresis curves with calculated ones, we chose, for each transition, a set of 10 values of K^* (corresponding to choosing 10 different widths of domains). We used equal volumes of domains for each value of K^*, so that the resulting fit was made with what appeared to be a set of steps, each of the same length, but at different heights from each other (Figs. 7–10). There was no attempt to ap-

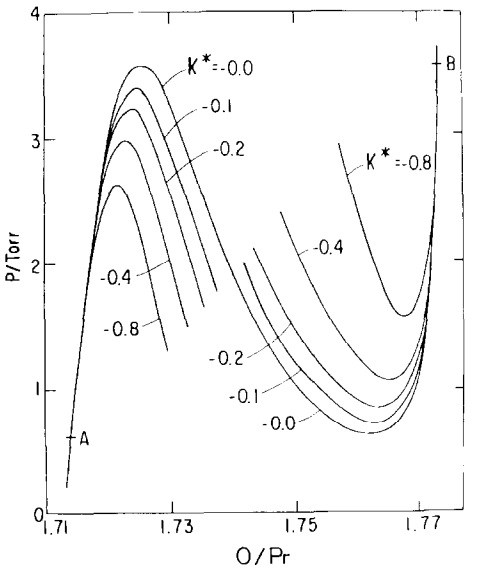

FIG. 4. Effect of various values of K^* on pressure versus concentration curves at 550°C.

portion amounts of different domains in a manner that would more closely approximate their real distribution, as this was a task more appropriate to the case of interacting domains. Here, we simply set out to examine more closely the effect of using a set of domains of different values of K^* (corresponding to different domain widths) to model the transition. (In the next section, the distribution of domain sizes is specified by a distribution function.)

The second parameter mentioned above, x_e, is a "system" parameter, and is the same for all domains in a given phase. The physical meaning of x_e is the equilibrium concentration, and as such there are two values used for x_e; one for phase A and another for phase B. One way to choose the x_e values would be to find the concentration values corresponding to points a and b on Fig. 2, which are the points at which equilibrium transitions would take place. A simpler approach is to choose the concentration values labeled c and d on Fig. 2, where c is at a pressure equal to the minimum on the van der Waals curve, and d is at a pressure equal to the maximum on the curve. Thus, for the forward transition, x_e is the point corresponding to point c on the pressure/concentration curve for the appropriate temperature. For the reverse transition, x_e is chosen as the concentration corresponding to point d on the same curve. The two approaches yield very similar values for x_e, and the second approach has the advantage that in the transition region, the absolute value of the difference $x - x_e$ is always increasing as the transition proceeds.

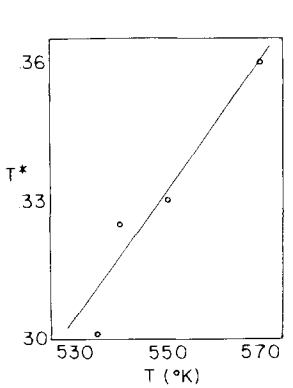

FIG. 5. Best fit values and least-square fit for T^* versus $10^3/T$ (K^{-1}).

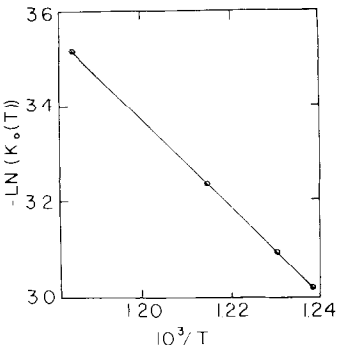

FIG. 6. Best fit values and least-square for ln $K_0(T)$ versus $10^3/T$) (K^{-1}).

For each of the four experimental curves worked with, we found values for T^* and $K_0(T)$ that would give the best fit of the calculated curve to the experimental one. (In comparing the fits of the endpoints of the calculated curves with the experimental ones, we are referring in each case to points on the lower left and upper right of each curve.) It was, of course, quite possible to find values for the pairs of parameters T^* and $K_0(T)$ which resulted in exact matches to the endpoints in each of Figs. 7–10. However, this would have resulted in using unrelated values of parameters. The relationship between ln $K_0(T)$ and $1/T$ is linear (Eq. (2.16)). The relationship between T^* and T is linear in terms of T, but there is also an inverse dependence of T^* on ε_i (Eq. (2.18)). Let us assume that ε_i varies linearly with T, that is: $-\varepsilon_i/k_B = (b + T)/a$. T^* may then be approximated as a first-order function of $1/T$,

$$T^* = a(1 - b/T). \qquad (2.19)$$

Employing a least-square fit of those values which gave best fits to the experimental

data, the values for the parameters were found to be 1.579 for a and 650.6 for b.

The relationship between ln $K_0(T)$ and $1/T$ should also be linear, as indicated by Eq. (2.16). Using the values of $K_0(T)$ that gave best fits to the experimental data at $T = 550$ and 570°C, extrapolated values were chosen for $K_0(T)$ at $T = 540$ and 535°C. This approach gave better overall results than a least-square fit of all best fit values for $K_0(T)$. It may also be worthy of note that the T^* values for $T = 550$ and 570°C were much closer to the least-square values of T^* than for $T = 540$ and 535°C. This indicates that there are either some subtle irregularities in the data for the four isothermal experimental runs, or that the linear approximations for T^* and $K_0(T)$ are insufficient to completely describe the system. Plots of the best fit values and the least-square values of T^* and ln $K_0(T)$ versus $1/T$ are shown in Figs. 5 and 6.

Once T^*, $K_0(T)$, and x_e values have been determined for a given experimental curve, the distribution of domain sizes had to be chosen to make the best possible fit to the given experimental data. In making this choice, the distribution of domain sizes is assumed to be the same for both the forward and reverse transitions (*9, 10*). Since it is conceivable that the K^* value for a domain undergoing a transition in the forward direction could be different from the K^* value for the same domain undergoing the reverse transition, the difference in potential K^* values was allowed for by introducing a final parameter, C, such that K^* (forward transition) = CK^* (reverse transition), where C is a constant. The number of domains of each size were chosen so that the slope of the theoretical fit was as close as possible to the experimental curve. Figures 7 to 10 show the theoretical fits to the experimental data. Table I summarizes the values chosen for T^*, $K_0(T)$, x_e, and C. Table II lists the values of K^* used for each calculated fit, as well as the volume of domains of each size used. It should be noted that from the K^* and ξ_i values, K/w^2 can be determined.

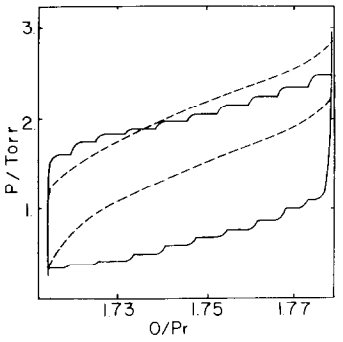

FIG. 8. Calculated fit to the hysteresis curve at 540°C, using 10 sets of noninteracting domains. —, calculated fit; ---, experimental.

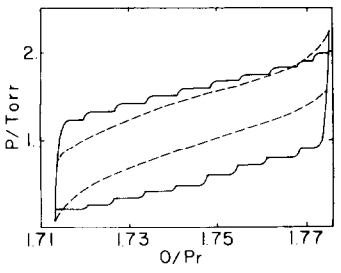

FIG. 7. Calculated fit to the hysteresis curve at 535°C, using 10 sets of noninteracting domains. —, calculated fit; ---, experimental.

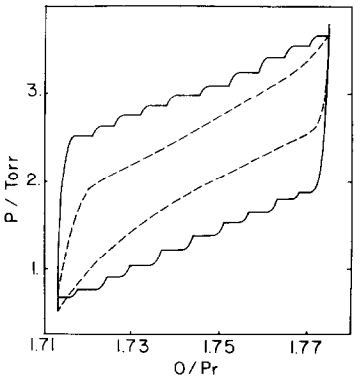

FIG. 9. Calculated fit to the hysteresis curve at 550°C, using 10 sets of noninteracting domains. —, calculated fit; ---, experimental.

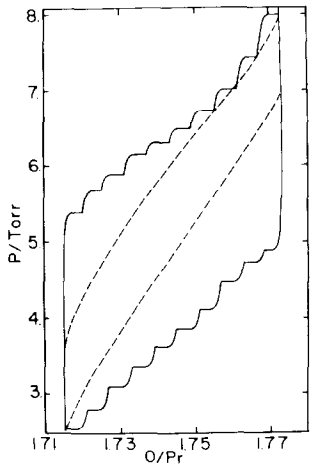

FIG. 10. Calculated fit to the hysteresis curve at 570°C, using 10 sets of noninteracting domains. —, calculated fit; ---, experimental.

TABLE II

VOLUME AND K^* FOR NONINTERACTING DOMAINS FOR HYSTERESIS FIT

535°C		540°C		550°C		570°C	
$-K^*$	V	$-K^*$	V	$-K^*$	V	$-K^*$	V
0.01	3	0.01	6	0.01	4	0.01	6
0.1	4	0.1	7	0.1	6	0.1	6
0.2	6	0.2	7	0.2	6	0.2	6
0.4	7	0.4	7	0.4	7	0.3	6
0.6	7	0.6	7	0.6	7	0.4	6
0.8	7	0.8	7	0.8	7	0.5	6
1.2	7	1.0	7	1.0	6	0.6	6
1.6	7	1.2	6	1.2	6	0.8	6
1.8	7	1.6	6	1.4	5	1.0	5
2.2	6	2.0	5	2.0	5	1.2	5

C. A Theoretical Model for the Kinetics of the Phase Transition

The kinetics of the solid state phase transition may be treated by using the free energy expression obtained in the hysteresis treatment. According to the theory of irreversible thermodynamics, for a system in a state not far from equilibrium the rate of change of the order parameter, a_i can be calculated from the free energy by (*13*)

$$\frac{\partial a_i}{\partial t} = \sum_j q_{ij} \frac{\partial \bar{G}}{\partial a_j}, \tag{2.20}$$

TABLE I

PARAMETER VALUES FOR CALCULATED HYSTERESIS CURVES

Item	Temperature (°C)			
	535	540	550	570
T^* (best fit)	0.301	0.325	0.330	0.360
T^* (least square)	0.3078	0.3156	0.3310	0.3606
$K_0(T)$ (best fit)	0.04380	0.04365	0.03893	0.02397
$K_0(T)$ (least square)	0.04837	0.04495	0.03893	0.02950
x_{e1}	0.0641	0.0688	0.0791	0.1037
x_{e2}	0.9580	0.9523	0.9396	0.9103
C	1	1	2	2

where q_{ij} represents the kinetic coefficients and $\bar{G}$ represents the molar free energy. This implies that the driving force for the change of the order parameter a_i is $\partial\bar{G}/\partial a_j$. In this case, the order parameter is identified as the mole fraction of oxygen atoms, x. This yields

$$\frac{\partial x}{\partial t} = q \frac{\partial \bar{G}}{\partial x}. \tag{2.21}$$

If $\bar{G}$ is obtained from the hysteresis treatment of the previous section, then

$$\bar{G} = \xi' x + \xi_i x^2 + \frac{Kx}{w^2}(x - x_e)^2 + k_B T[x \ln x + (1 - x)\ln(1 - x)], \tag{2.22}$$

where $\xi' = \xi_0 - (\frac{1}{2})\mu_{O_2}$.

Substituting Eq. (2.22) into Eq. (2.21) yields

$$\frac{\partial x}{\partial t} = q\left[\xi' + 2\xi_i x + \frac{K}{w^2}(x - x_e)(3x - x_e) + k_B T \ln\left(\frac{x}{1 - x}\right)\right]. \tag{2.23}$$

Notice that in thermal equilibrium, the following relation may be derived from Eqs. (2.13) and (2.14),

$$\xi' + 2\xi_i x_0 + \frac{K}{w^2}(x_0 - x_e)(3x_0 - x_e) + k_B T \ln\left(\frac{x_0}{1 - x_0}\right) = 0. \quad (2.24)$$

From Eqs. (2.23) and (2.24), one can obtain

$$\frac{d\Delta x}{dt} = q[2\xi_i \Delta x + k_B T \ln(1 + \Delta x/x_0)/(1 - \Delta x/(1 - x_0) + \frac{K}{w^2}\Delta x(3\Delta x + 6x_0 - 4x_e)], \quad (2.25)$$

where $\Delta x = x - x_0$. Here, x_0 refers to the equilibrium concentration x for a given pressure. Expanding the right-hand side of Eq. (2.25) in a power series of x yields the first-order approximation

$$\frac{d\Delta x}{dt} = -k_1 \Delta x, \quad (2.26)$$

where

$$k_1 = -q\left[2\xi_i + \frac{k_B T}{x_0(1 - x_0)} + \frac{K}{w^2}(6x_0 - 4x_e)\right]. \quad (2.27)$$

Further expansion yields the second-order approximation

$$\frac{d\Delta x}{dt} = -k_r \Delta x = -(k_1 + k_2 \Delta x)\Delta x, \quad (2.28)$$

where

$$k_2 = -q\left[\frac{3K}{w^2} + \frac{(x_0 - 0.5)k_B T}{x_0^2(1 - x_0)^2}\right]. \quad (2.29)$$

D. Application of the Kinetics Model to the Pr_7O_{12}–Pr_9O_{16} Phase Transition

In this section, the previously derived theoretical model for the kinetics of the phase transition are applied to data taken by Inaba *et al.* (*11*).

From Eqs. (2.27) and (2.28) one can see that the rate constant k_r depends on x_0, the equilibrium oxygen atom concentration, which in turn depends on the O_2 pressure P_{O_2} as discussed in the previous section. Expressing Eq. (2.27) in reduced variables yields

$$k_1' = -\frac{k_1}{qk_B T} = -\frac{2}{T^*} + \frac{1}{x_0(1 - x_0)} + \frac{\bar{K}^*}{T^*}(6x_0 - 4x_e), \quad (2.30)$$

where $\bar{K}^*$ represents an average value of K^* since the kinetic measurements involve the system as a whole and not individual domains.

Equation (2.29) becomes

$$k_2' = \frac{-k_2}{qk_B T} = 3\frac{\bar{K}^*}{T^*} + \frac{(x_0 - 0.5)}{x_0^2(1 - x_0)^2}, \quad (2.31)$$

and in reduced variables, Eq. (2.28) becomes

$$\frac{d\Delta x}{dt'} = -k_r' \Delta x = -(k_1' + k_2' \Delta x)\Delta x, \; t' = -qk_B T t. \quad (2.32)$$

In Fig. 11, the comparison of both first- and second-order theoretical results with the experimental results for the oxygen pressure dependence k_r is shown. It can be seen from this figure that for a given temperature k_r can vanish at a particular oxygen pressure. For the second-order calcula-

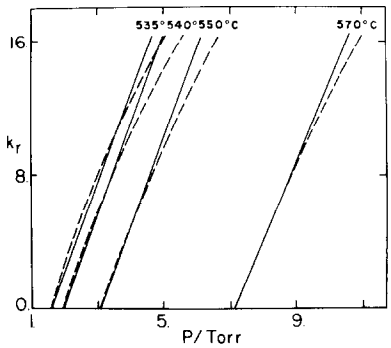

FIG. 11. Calculated fit to the experimental rate constants, k_r, obtained by Inaba *et al.* (*11*), (---) first-order approximation; (—) second-order approximation, which is an excellent fit to the experimental data (i.e., this curve also represents the experimental curve).

tions, it was necessary to solve iteratively for the Δx that yielded the best fit of Eq. (2.32) to the experimental results.

The coefficient q has also been determined, and has been found to be a function of temperature. Each isothermal study yields one value of q. The four q values obtained from the experimental work of Inaba *et al.* (*11*) were fit by an equation of the Arrhenius form

$$q = A \exp(-a/T) \tag{2.33}$$

where a was found to be 3.58×10^4 K^{-1}, and A was 1.15×10^{13} sec^{-1}. The values for $q(T)$ and $\bar{K}^*$ are summarized in Table III.

The theoretical fit to the experimental kinetic data of Inaba *et al.* was found to be quite good for the second-order approximation for k_r. While the constant $\bar{K}^*$ was chosen in each case to cause the P_{O_2} intercept of the theoretical curve of k_r versus P_{O_2} to coincide with the experimental one, one can note that it is similar in both sign and magnitude to the values of K^* chosen for the thermodynamic fits. The P_{O_2} intercept for the oxidation reaction represents the minimum P_{O_2} that causes the reaction to take place; this can be seen by minimizing P_{O_2} with respect to x using Eq. (2.15).

III. A Theoretical Model for a Solid State Phase Transition Using Interacting Domains

In approaching a study of a system with interacting domains, it is necessary to consider the nature of domain interactions (*17*). The interaction energy proposed here is based on the idea of an interfacial free energy between two domains of unlike composition. The local free energy for an area in the interfacial region is viewed as a function of the local concentration of oxygen atoms, the concentration gradient, and the derivatives of the gradient. The concentration gradient is taken across the width of the domain interface. The free energy per excess atom, g, may be written as a Taylor expansion about g_0, the free energy per excess atom in an area of uniform concentration, in a manner similar to that used in the previous section. Integrating g over the interfacial region, we obtain (*18*)

$$G = G_0(x) + G_{int}(x) \tag{3.1}$$

where $G_0(x)$ is simply the free energy expression for a domain, as derived in Section II. G_{int}, the interfacial free energy, is composed of two terms

$$G_{int} = C(X_2^3 - x_2^2 x_1 - x_2 x_1^2 + x_1^3) + \frac{D}{2}(x_2^2 - 2x_2 x_1 + x_1^2) \tag{3.2}$$

where x_1 is the concentration in the domain being considered and x_2, the concentration in its nearest-neighbor. C and D are constants depending on the size of the domain.

The expression for the interfacial free energy is symmetric; that is, the same results are obtained if x_1 and x_2 are interchanged. This agrees with the expectation that an interfacial region will have the same free energy whether the integration is taken from the left-to-right or right-to-left sides of the region. Further, if two nearest-neighbor domains have the same excess atom concentration, the interfacial free energy is zero. In the case where the interfacial free energy is not zero, half the free energy is assigned to one domain, and half to its nearest-neighbor.

Taking the derivative of Eq. (3.2) with

TABLE III

VALUES FOR KINETICS PARAMETERS

T (°C)	$-q(T)k_B$	$\bar{K}^*$	P_{O_2}(intercept) (Torr)
535	0.642×10^{-6}	1.5572	1.50
540	0.830×10^{-6}	1.3892	2.00
550	1.432×10^{-6}	1.1147	3.09
570	4.022×10^{-6}	0.7051	7.10

respect to x_1 yields the interfacial term of the chemical potential for a domain,

$$\mu_{int} = \frac{\partial G_{int}}{\partial x_1} = C(3x_1^2 - 2x_1x_2 - x_2^2) + D(x_1 - x_2). \quad (3.3)$$

This expression is not symmetrical with respect to x_1 and x_2, which is as expected. For a domain with a low concentration x, μ_{int} should be negative, indicating that the excess atoms have a lower escaping tendency. For a domain with a high concentration of excess atoms, μ_{int} should be positive, reflecting an increased escaping tendency for those atoms.

The effect of the interfacial chemical potential on the pressure versus concentration curve may be seen by viewing the total chemical potential for a domain as the sum of the chemical potential for a domain as calculated in Section II and two interfacial chemical potential terms, one each for the right- and left-hand side interactions:

$$\mu = \mu_0 + \mu_{int}(\text{RHS}) + \mu_{int}(\text{LHS}). \quad (3.4)$$

As before, the chemical potential for a domain is set equal to half the chemical potential for the external oxygen,

$$\tfrac{1}{2}\mu_{O_2} = \tfrac{1}{2}\mu^0_{O_2} + \tfrac{1}{2}k_BT \ln P_{O_2} = \mu_0 + \mu_{int}(\text{RHS}) + \mu_{int}(\text{LHS}). \quad (3.5)$$

The equation is now expressed in terms of P_{O_2},

$$P_{O_2}K_0^2(T) = \exp\left[\frac{2\mu_0 - 2\xi_0}{k_BT}\right] \exp\left[\frac{2\mu_{int}(\text{RHS})}{k_BT}\right] \exp\left[\frac{2\mu_{int}(\text{LHS})}{k_BT}\right]. \quad (3.6)$$

Let $\exp(2\mu_{int}/k_BT) = E_i$. A domain in phase A, with a low value for x, will have μ_{int} less than zero, and hence E_i less than one. The effect of a nearest-neighbor in B on a domain in A will be to reduce the value of P_{O_2} for a given value of x, because the entire curve will be multiplied by a number less than one (E_i). Thus, the domain will undergo a transition to phase B at a lower pressure than it would if it had no nearest-neighbor in B, because the maximum in its pressure versus concentration curve (the pressure at which it undergoes transition) will have been lowered.

The effect of a nearest-neighbor in A on a domain in B will be to cause it to undergo a transition at a slightly higher pressure than it otherwise would have, because the pressure versus concentration curve will have been multiplied by a value for E_i greater than one.

Thus, the overall effect of the interactions may be summarized as follows: If the pressure is being slowly increased, a domain in A will undergo transition at a slightly lower pressure than it normally would if it has a nearest-neighbor in B. If it has two nearest-neighbors in phase B, it will undergo the transition at a still lower pressure. This will appear to have the effect of having domains "grow," that is, the nearest-neighbors of a domain that has undergone a transition are more likely to undergo transition than domains that do not have a nearest-neighbor in B. A similar effect will be observed if the pressure is slowly decreased from a value at which all or most of the domains are in B; that is, those domains that have nearest-neighbors in A will undergo transitions slightly before those that do not have nearest-neighbors in A.

The theoretical results (*18*) can be applied to the solid iota–zeta phase transition of praseodymium oxide. The praseodymium oxide system is considered to be composed of a number of domains of various lengths, but each having the width and height of one unit cell. Two arrangements for the domains are considered; a one-dimensional array and a two-dimensional (square) array. The numbers of different lengths of domains were chosen to fit the experimental data, and were invariant for all calculations.

The different lengths of domains allowed different concentration gradients to be set up in the domains. These concentration gradients were presumed to terminate in a defect or to be caused by various diffusion gradients. It was presumed that the length of a domain was invariant during the transition to the high oxygen concentration phase B and the reverse transition to the low-concentration phase A (hereafter referred to as forward and reverse transitions). It was also presumed that the material behind the domain (continuing down the length of the column that the domain originated) would rapidly undergo transition so as to be in the same phase as the domain at the head of the column. This is in accord with the results of high-resolution transmission electron microscopy images of the phase transition, which show domains nucleating or growing slowly across the face of the system exposed to the external oxygen, but growing rapidly in length once begun (*15*). Although the system studied via HRTEM is not under the same conditions used during the phase transition studied here, the physical structure of the praseodymium oxide system does not make such an assumption unreasonable. The result of this assumption is that the volume of the system in a phase is proportional to the number of domains in that phase. For both the one-dimensional and two-dimensional models, an exponential function was used to apportion the numbers of domains of various sizes. In this manner, the number of very small domains is much larger than the number of very large domains, as would seem physically reasonable. This approach yields a reasonably good match with the experimental data, especially at the end of the forward transition (when only the very large domains are completing their transition to the new phase).

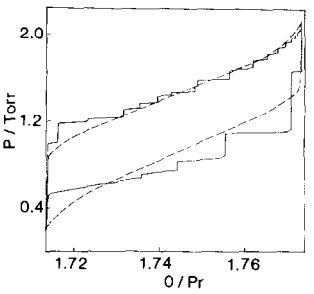

FIG. 12. Calculated fit (—) to the experimental hysteresis curve (---) for the Pr_7O_{12}–Pr_9O_{16} phase transition. For this figure, the temperature is 535°C, and the parameters used to achieve the fit were $T^* = 0.3360$ and $K_0(T) = 0.04899$.

Values for T^*, $K_0(T)$, x_e, and K^* were redetermined for the application of the interacting domain model to the iota–zeta praseodymium oxide phase transition, and are summarized in Table IV. T^* and $K_0(T)$ were found by linearizing the best fits to the experimental data for T = 535, 550, and 570°C. It was judged that the data for T = 540°C were most deviating in attempts to use a linear fit of T^* and ln $K_0(T)$ to $1/T$. The values for x_e were chosen to give the best fits to the experimental data, as application of the rule of equal area gave values of x_e that yielded very poor fits. K was kept at −40 for all forward transitions, and at approximately −10 for the reverse transitions. If larger magnitudes of K were used for the reverse transition, the minima, instead of steadily increasing with decreased length of domains, would double-back and start to decrease. The overall result, however, is that the fit of the reverse hysteresis

TABLE IV

PARAMETERS USED IN APPLICATION OF INTERACTING DOMAIN MODEL TO THE IOTA–ZETA PHASE TRANSITION

Parameters relating to theoretical treatment				
T(°C)	535	540	550	570
T^*	0.3360	0.3394	0.3461	0.3590
$K_0(T)$	0.04899	0.04477	0.03748	0.02660
x_{e1}	0.0344	0.0339	0.0397	0.0536
x_{e2}	0.9701	0.9695	0.9659	0.9599

curve to the experimental is not as good as the fit of the forward hysteresis curve.

Two similar programs were used to model the forward and reverse phase transitions under the assumptions of a one-dimensional and a two-dimensional array of domains, respectively.

Figures 12–15 show the fits to the four isothermal systems considered for two-dimensional domain array models. The results for the one-dimensional array models are very similar and thus are not shown. The programs were run on a Hewlett–Packard 3000 Series II, and the plots in Figs. 12–15 were drawn via a subroutine on a Zeta Plotter 100 Series.

It may be noted that the fits to the experimental data obtained here are much better than those of Section II. This is in part due to the fact that under the model considered in Section II, the pressure at which a domain underwent the forward transition (P_1) had to be greater than or equal to the pressure at which it underwent the reverse transition (P_2). Otherwise, if $P_2 > P_1$, the domain, upon undergoing transition, would immediately become unstable in the new phase and promptly revert back to the original phase A. Thus, for the largest domain under consideration, the value for K^* had to be such that $P_1 > P_2$, which affected the shape of the curve.

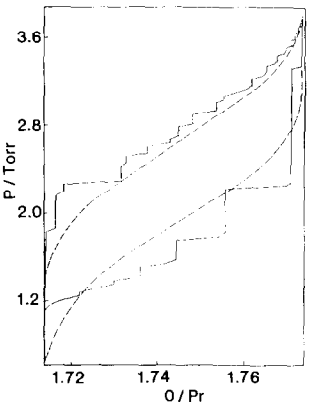

FIG. 14. Calculated fit (—) to the experimental hysteresis curve (---) for the Pr_7O_{12}–Pr_9O_{16} phase transition. For this figure, the temperature is 550°C, and the parameters used were $T^* = 0.3461$ and $K_0(T) = 0.03748$.

When a domain undergoes a transition, the new phase affects not only the domain but also the entire length of the column after it. It is assumed that the concentration gradient establishing the new domain in phase B does not come into existence until the pressure is first reduced slightly.

When the two-dimensional approach is used, the 603 domains comprising the model system were viewed as approxi-

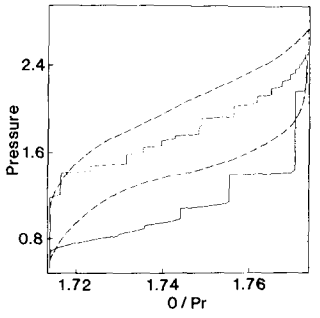

FIG. 13. Calculated fit (—) to the experimental hysteresis curve (---) for the Pr_7O_{12}–Pr_9O_{16} phase transition. For this figure, the temperature is 540°C, and the parameters used were $T^* = 0.3394$ and $K_0(T) = 0.04477$.

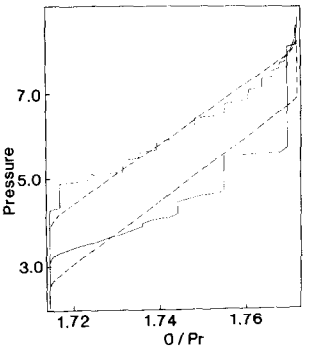

FIG. 15. Calculated fit (—) to the experimental hysteresis curve (---). For this figure, $T = 570$°C, $T^* = 0.3590$, and $K_0(T) = 0.02660$.

mately a 25 × 24 rectangular array with 1206 bonds shared between nearest-neighbors (the bonds to "imaginary" nearest-neighbors are included in the array, as the program does not make any attempt to restrict the bonds that can be formed due to geography).

From Figs. 7–10 one can see that the introduction of independent domains does improve the fit between theory and experiment (cf. also Fig. 3) but the agreement is still not satisfactory. The introduction of interaction between domains (Figs. 12–15) is clearly important in treating the hysteresis of phase transitions in solids.

In concluding this paper, it should be noted that a general formulation of the kinetics of solid state phase transitions is not available. In this paper we attempt, in an ad hoc manner, to show that for systems that exhibit hysteresis in phase transitions (at least for Pr_7O_{12}–Pr_9O_{16}) one can determine the kinetics of the corresponding phase transition from the free energies.

Acknowledgments

We are happy to acknowledge support from the National Science Foundation through Grant DMR78-05722. We also express our appreciation for many helpful conversations with Dr. H. Inaba.

References

1. S. G. PIMPOLE, *J. Pure Appl. Phys.* **12,** 565 (1974); J. A. BALDWIN, *J. Appl. Phys.* **43,** 1063 (1971).
2. R. SENGUPTA AND A. GUHA, *Indian J. Phys.* **46,** 528 (1972); A. GUHA AND S. H. LIN, *in* "The Chemistry of Extended Defects in Non-metallic Solids" (L. Eyring and M. O'Keeffe, Eds.), North-Holland, Amsterdam (1970).
3. D. H. EVERETT, "The Solid-Gas Interface," Dekker, New York (1967) Vol. 2, pp. 1055–1133; L. A. G. AYLMORE, *J. Colloid Interface Sci.* **46,** 410 (1974).
4. A. T. LOWE AND L. EYRING, *J. Solid State Chem.* **72,** 2030 (1968).
5. C. L. CREEL AND J. ROSS, *J. Chem. Phys.* **65,** 3779 (1976).
6. E. NEUMANN, *Angew. Chem. Int. Ed.* **12,** 356 (1973).
7. D. R. KNITTEL, S. P. PACK, S. H. LIN, AND L. EYRING, *J. Chem. Phys.* **67,** 134 (1977); D. R. KNITTEL, Ph.D. dissertation, Arizona State University (1977).
8. S. M. MA, S. H. LIN, AND H. EYRING, *Proc. Nat. Acad. Sci. USA* **75,** 4664 (1978).
9. D. H. EVERETT AND W. I. WHITTON, *Faraday Soc.* **48,** 749 (1952); D. H. EVERETT AND F. W. SMITH, **50,** 187 (1954); D. H. EVERETT, **50,** 1077 (1954).
10. J. A. ENDERBY, *Trans. Faraday Soc.* **51,** 835 (1955).
11. H. INABA, S. P. PACK, S. H. LIN, AND L. EYRING, *J. Solid State Chem.* **33,** 295 (1980).
12. J. W. CAHN AND J. E. HILLIARD, *J. Chem. Phys.* **28,** 258 (1958).
13. S. R. DE GROOT, "Thermodynamics of Irreversible Processes," North-Holland, Amsterdam (1951).
14. R. KIKUCHI, *Suppl. Prog. Theor. Phys.* **35,** 1 (1966).
15. L. EYRING, *in* "Nonstoichiometric Oxides" (O. Toft Sørensen, Ed.), Chap. 7, Academic Press, New York (1981).
16. E. A. GUGGENHEIM, "Mixtures," Oxford Univ. Press (Clarendon), London/New York (1952).
17. R. KIKUCHI AND S. G. BRUSH, *J. Chem. Phys.* **47,** 195 (1967).
18. M. B. LANGLEY, Ph.D. dissertation (a.k.a. A. Maren), Arizona State University (1981).